Author(s): Ranta, Mikaela & Hinkkanen, Marko

Title: Online identification of parameters defining the saturation characteristics of induction machines

Year: 2013

Version: Post print

Please cite the original version:

Ranta, Mikaela & Hinkkanen, Marko. 2013. Online identification of parameters defining the saturation characteristics of induction machines. IEEE Transactions on Industry Applications. Volume 49, Issue 5, P. 2136-2145. ISSN 1939-9367 (electronic). ISSN 0093-9994 (printed). DOI:10.1109/TIA.2013.2261793.

Online Identification of Parameters Defining the Saturation Characteristics of Induction Machines

Mikaela Ranta and Marko Hinkkanen, *Member, IEEE*
Aalto University School of Electrical Engineering
P.O. Box 13000, FI-00076 Aalto, Finland

***Abstract*—The induction machine model parameters need to be estimated with good accuracy to ensure a good performance of the drive. Due to the magnetic saturation, the inductances vary as a function of the flux level. The magnetizing curve can be identified at standstill, but more accurate results are obtained if the identification is performed as the machine is running. In this paper, the magnetic saturation is modelled using a power function, and adaptation laws for the function parameters are proposed. The adaptation method is implemented in the control system of a sensorless drive. Experimental results on a 2.2-kW machine show that the identification of the stator inductance is rapid and the accuracy is good.**

***Index Terms*—Induction motor, magnetic saturation, parameter estimation, sensorless control.**

I. Introduction

The control of an electric drive is based on a model of the machine. In order to achieve a good performance, the model parameters need to be identified with good accuracy. Particularly, when the flux-weakening region is entered or the flux is controlled in order to optimize the drive (e.g., a loss-minimizing algorithm is applied), the dependency of the inductances on the magnetic saturation should be known.

The magnetic saturation is commonly taken into account by modelling the magnetizing inductance as a function of the magnetizing flux or current. Hence, the saturation can be modelled with a rather simple function and the resulting inductance estimate is accurate enough in most cases. In machines having closed or skewed rotor slots, the load might slightly affect the saturation characteristics due to partly common iron paths of the magnetizing and leakage fluxes [1], [2]. The phenomenon can be investigated by finite element analysis and by measurements in a laboratory environment where the speed and load can be freely varied. However, in real-life applications, the identification of the magnetizing curve becomes difficult if the influence of the load is taken into account.

An extensive review of parameter identification techniques for induction machines was presented in [3]. Ideally, the magnetic characteristics are identified at standstill during the self-commissioning of the drive without any auxiliary measurements. A great number of different identification methods have been developed for this purpose [4]–[10]. Methods based on a flux reversal when single-phase excitation is used have been proposed by several authors [4]–[6]. In [4], the identification was based on a recursive least-squares algorithm while the magnetizing curve was obtained by integration of the stator voltage data in [5], [6]. In [7], the magnetizing inductance was identified by applying a number of voltage steps. An iterative identification method of the magnetizing inductance was proposed in [8] using sinusoidal single-phase voltage excitation. In [9], sinusoidal excitation at two frequencies was used, and the magnetizing inductance was obtained from the impedance seen at the stator terminals. In [10], the magnetizing curve was modelled by a polynomial function, and the parameters of the function were obtained based on data from single-phase excitation at standstill using a recursive least-squares algorithm. As the identification is performed at standstill in the proposed methods, the load does not need to be disconnected. However, the obtained magnetizing inductance is less accurate than the result obtained when the machine is supplied by a rotating stator voltage [8]. Identification methods at standstill are also prone to voltage measurement errors as low voltage levels have to be used [11].

The magnetizing curve can also be identified as the machine is running. In [11], a function based on the stator current and stator voltage integral was used to identify the magnetizing inductance. An acceleration test was used in [12] to identify the machine parameters. The maximum likelihood estimation was used, and the method requires measurement of the speed. In [13], a method for identifying the magnetizing curve function was presented, but the method was only able to identify one parameter. A speed-sensorless method was proposed in [14], where a Luenberger observer was used for the inductance identification.

To store the magnetizing curve, a look-up table can be used, or a function can be fitted to the data unless the function parameters are directly identified as in [10]. However, look-up tables require a lot of memory, and data fitting easily becomes time-consuming. An alternative is to use neural networks [12], [14]. A neural network is a powerful tool to model a nonlinear behaviour of a process. However, it requires training data for a sufficient amount of operating points and might become unnecessarily complicated. It is also possible to update the inductance during the operation of the drive [15]. In this case, a magnetizing curve does not necessarily need to be stored in the memory. On the other hand, continuous adaptation of the inductance might lead to poor dynamic behaviour of the drive. Furthermore, in sensorless drives, the adaptation of the inductance is practically impossible since the speed has to be estimated and adaptation of the stator resistance might be necessary in order to ensure stability at low speeds.

In this paper, the stator inductance is modelled as a function of the stator flux using a simple power function. A method to identify the power function parameters during the self-

commissioning of a sensorless drive is proposed. By varying the flux, the parameters of the saturation function can rapidly be identified, and the stator inductance can be calculated in every operating point without using any additional data fitting method. The method requires the machine to be allowed to rotate during the identification process. As the correct function parameters are obtained, the adaptation mechanism can be turned off without losing control accuracy when the flux varies later on. Hence, good dynamic performance of the drive can be ensured. The adaptation method is combined with a leakage inductance identification method based on signal injection in order to ensure good results also when a no-load condition cannot be reached during the stator inductance identification process. Simulations and laboratory experiments are performed in order to investigate the proposed adaptation method. The results show that the convergence of the parameter estimates is fast and the accuracy is good.

II. Induction Machine Model

Real-valued space vectors will be used; for example the stator current is $\boldsymbol{i}_\mathrm{s} = \begin{bmatrix} i_\mathrm{sd} & i_\mathrm{sq} \end{bmatrix}^\mathrm{T}$ and its magnitude is denoted by

$$i_\mathrm{s} = \|\boldsymbol{i}_\mathrm{s}\| = \sqrt{i_\mathrm{sd}^2 + i_\mathrm{sq}^2} \tag{1}$$

The identity matrix is $\mathbf{I} = \left[\begin{smallmatrix} 1 & 0 \\ 0 & 1 \end{smallmatrix}\right]$ and the orthogonal rotation matrix is $\mathbf{J} = \left[\begin{smallmatrix} 0 & -1 \\ 1 & 0 \end{smallmatrix}\right]$. The induction machine can be described by the classical T model, the inverse-Γ model or the Γ model. In the following, the models are shortly presented.

A. T model

The induction machine is traditionally described by the T model shown in Fig. 1(a). In synchronous coordinates rotating at the angular frequency ω_s, the machine can be described by

$$\frac{\mathrm{d}\boldsymbol{\psi}_\mathrm{s}}{\mathrm{d}t} = \boldsymbol{u}_\mathrm{s} - R_\mathrm{s}\boldsymbol{i}_\mathrm{s} - \omega_\mathrm{s}\mathbf{J}\boldsymbol{\psi}_\mathrm{s} \tag{2a}$$

$$\frac{\mathrm{d}\boldsymbol{\psi}_\mathrm{r}}{\mathrm{d}t} = -R_\mathrm{r}\boldsymbol{i}_\mathrm{r} - \omega_\mathrm{r}\mathbf{J}\boldsymbol{\psi}_\mathrm{r} \tag{2b}$$

where $\boldsymbol{u}_\mathrm{s}$ is the stator voltage, $\boldsymbol{i}_\mathrm{s}$ the stator current, and $\boldsymbol{i}_\mathrm{r}$ the rotor current. The stator flux is denoted by $\boldsymbol{\psi}_\mathrm{s}$ and the rotor flux by $\boldsymbol{\psi}_\mathrm{r}$. The stator resistance and rotor resistance are R_s and R_r, respectively. The angular slip frequency $\omega_\mathrm{r} = \omega_\mathrm{s} - \omega_\mathrm{m}$, where ω_m is the electrical rotor speed. The stator flux and rotor flux are given by

$$\boldsymbol{\psi}_\mathrm{s} = L_\mathrm{s}\boldsymbol{i}_\mathrm{s} + L_\mathrm{m}\boldsymbol{i}_\mathrm{r}, \qquad \boldsymbol{\psi}_\mathrm{r} = L_\mathrm{m}\boldsymbol{i}_\mathrm{s} + L_\mathrm{r}\boldsymbol{i}_\mathrm{r} \tag{3}$$

respectively. The magnetizing inductance is L_m, the stator inductance $L_\mathrm{s} = L_{\mathrm{s}\sigma} + L_\mathrm{m}$, and the rotor inductance $L_\mathrm{r} = L_{\mathrm{r}\sigma} + L_\mathrm{m}$.

B. Inverse-Γ Model

The T model is over-parametrized, i.e., the induction machine can be described using less parameters than in the T model. The leakage inductance can be totally referred to the stator side, leading to the inverse-Γ model shown in Fig. 1(b). The rotor voltage equation is now

$$\frac{\mathrm{d}\boldsymbol{\psi}_\mathrm{R}}{\mathrm{d}t} = -R_\mathrm{R}\boldsymbol{i}_\mathrm{R} - \omega_\mathrm{r}\mathbf{J}\boldsymbol{\psi}_\mathrm{R} \tag{4}$$

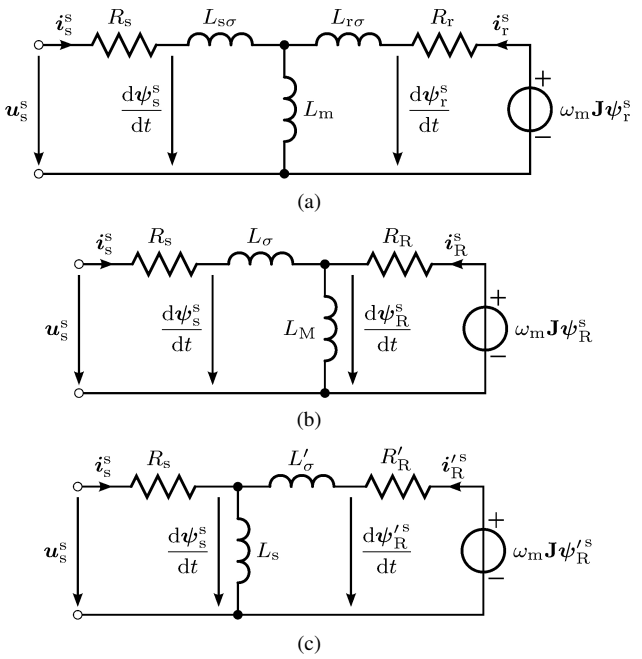

Fig. 1. Dynamic induction machine models in stator coordinates: (a) T model; (b) inverse-Γ model; (c) Γ model. The superscript s denotes stator coordinates.

The stator flux and rotor flux are given by

$$\boldsymbol{\psi}_\mathrm{s} = L_\sigma\boldsymbol{i}_\mathrm{s} + \boldsymbol{\psi}_\mathrm{R}, \qquad \boldsymbol{\psi}_\mathrm{R} = L_\mathrm{M}(\boldsymbol{i}_\mathrm{s} + \boldsymbol{i}_\mathrm{R}) \tag{5}$$

respectively, where L_σ is the leakage inductance and L_M the magnetizing inductance. The parameters of the inverse-Γ model can be obtained from the parameters of the T model by

$$L_\mathrm{M} = k_\mathrm{r}L_\mathrm{m}, \quad L_\sigma = L_{\mathrm{s}\sigma} + k_\mathrm{r}L_{\mathrm{r}\sigma}, \quad R_\mathrm{R} = k_\mathrm{r}^2 R_\mathrm{r} \tag{6}$$

where $k_\mathrm{r} = L_\mathrm{m}/L_\mathrm{r}$.

C. Γ Model

The inverse-Γ model is convenient in the control of the drive, but the magnetic saturation can be more easily modelled in the Γ model in Fig. 1(c). In the Γ model, the flux equations are

$$\boldsymbol{\psi}_\mathrm{s} = L_\mathrm{s}(\boldsymbol{i}_\mathrm{s} + \boldsymbol{i}'_\mathrm{R}), \qquad \boldsymbol{\psi}'_\mathrm{R} = \boldsymbol{\psi}_\mathrm{s} + L'_\sigma\boldsymbol{i}'_\mathrm{R} \tag{7}$$

The leakage inductance and rotor resistance of the Γ model are related to the parameters of the T model according to

$$L'_\sigma = \frac{L_{\mathrm{s}\sigma}}{k_\mathrm{s}} + \frac{L_{\mathrm{r}\sigma}}{k_\mathrm{s}^2}, \quad R'_\mathrm{R} = \frac{R_\mathrm{r}}{k_\mathrm{s}^2} \tag{8}$$

where $k_\mathrm{s} = L_\mathrm{m}/L_\mathrm{s}$. The rotor voltage equation changes in a similar manner as in the inverse-Γ model.

In the control of the machine, both the Γ model and the inverse-Γ model will be used. If the parameters of the Γ model are known, the parameters of the inverse-Γ model are obtained as

$$L_\mathrm{M} = kL_\mathrm{s}, \quad L_\sigma = kL'_\sigma, \quad R_\mathrm{R} = k^2 R'_\mathrm{R} \tag{9}$$

where

$$k = \frac{L_\mathrm{s}}{L_\mathrm{s} + L'_\sigma} \tag{10}$$

In the case of constant-valued parameters, the T model, inverse-Γ model, and Γ model are mathematically equivalent, i.e. the expressions (6), (8), and (9) for the conversions are valid also during transients. If the machine saturates, the models are no longer equivalent as the incremental inductances are not included,[1] but the conversions are still valid in steady state.

D. Magnetic Saturation

According to [16], the Γ model is most suitable for modeling the saturation of the induction machine, since the flux density in the stator is mainly dependent on the stator flux linkage. The stator inductance L_s and the leakage inductance L'_σ depend on the flux linkages (or the currents) due to the magnetic saturation. However, modeling the stator inductance L_s as a function of the stator flux typically suffices. In this paper, the stator inductance is modeled by a simple power function [17]:

$$L_\mathrm{s} = \frac{L_\mathrm{su}}{1 + (\beta\psi_\mathrm{s})^S} \tag{11}$$

where L_su is the unsaturated inductance, and S and β are nonnegative constants. No-load tests were performed on a 2.2-kW machine, and the stator inductance in (11) was fitted to the data in order to obtain the parameter values. The fitted stator inductance is shown in Fig. 2 together with measured stator inductance values. As can be seen, the model describes the saturation very well under no load.

However, the load might affect the saturation characteristics in machines having skewed [2] or closed rotor slots [1], [18]. As a result, both the stator inductance and the rotor leakage inductance are dependent on the rotor current [19]. The load-dependency of the inductances can be modeled according to [20]

$$L_\mathrm{s} = \frac{L_\mathrm{su}}{1 + (\beta\psi_\mathrm{s})^S + \frac{\gamma L_\mathrm{su}}{d+2}\psi_\mathrm{s}^c\psi_\sigma'^{d+2}} \tag{12a}$$

$$L'_\sigma = \frac{L'_{\sigma\mathrm{u}}}{1 + (\beta'\psi'_\sigma)^b + \frac{\gamma' L'_{\sigma\mathrm{u}}}{c+2}\psi_\mathrm{s}^{c+2}\psi_\sigma'^{d}} \tag{12b}$$

where the magnitude of the leakage flux is $\psi'_\sigma = ||\boldsymbol{\psi}'_\mathrm{R} - \boldsymbol{\psi}_\mathrm{s}||$ in accordance with Fig. 1(c). Based on (12a), the stator inductance is calculated at different values of the electromagnetic torque, and the influence of the torque is illustrated in Fig. 2. As the torque increases, the stator inductance decreases at low stator flux levels. The parameter values used in the figure are given in Table I. The parameters necessary for including the influence of the torque were obtained from [20], where the same machine as used in this paper was analysed under loaded conditions.

In this paper, the model in (11) is used since it has only three parameters. In Section IV-B, a method for identifying the parameters L_su and β is proposed, and S can be selected based on a priori information.

[1]The inverse-Γ rotor flux is $\boldsymbol{\psi}_\mathrm{R} = k_\mathrm{r}\boldsymbol{\psi}_\mathrm{r}$. The derivative of the conversion factor k_r should be included in order to make the rotor voltage equations (2b) and (4) equivalent in transients.

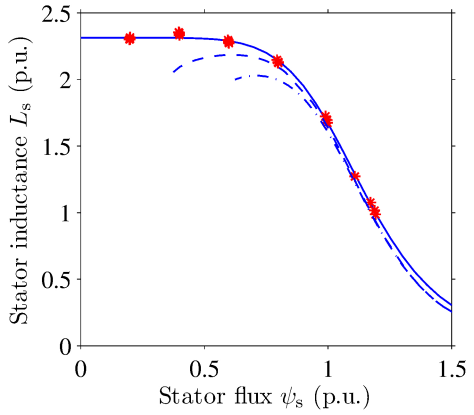

Fig. 2. Stator inductance as function of stator flux in a no-load condition (solid line) and as the torque equals half of rated value (dashed line) and rated value (dash-dotted line). Markers show the measured values from no-load tests on a 2.2-kW machine.

TABLE I
PARAMETER VALUES FOR THE INDUCTANCES OF A 2.2-KW MACHINE

L_su	β	S	$L'_{\sigma\mathrm{u}}$	β'	γ	b	c	d
2.31	0.87	7	0.22	0.51	3.20	1.0	0.0	0.0

III. OBSERVER

The reduced-order observer presented in [21] will be used, with the addition of adaptation of the stator inductance parameters L_su and β. The observer is based on the inverse-Γ model. Two back EMFs are used in the estimation of the rotor flux: the back EMF corresponding to the voltage model

$$\boldsymbol{e} = \boldsymbol{u}_\mathrm{s} - \hat{R}_\mathrm{s}\boldsymbol{i}_\mathrm{s} - \hat{L}_\sigma\frac{\mathrm{d}\boldsymbol{i}_\mathrm{s}}{\mathrm{d}t} - \hat{\omega}_\mathrm{s}\hat{L}_\sigma\mathbf{J}\boldsymbol{i}_\mathrm{s} \tag{13}$$

and the back EMF corresponding to the current model

$$\hat{\boldsymbol{e}} = \hat{R}_\mathrm{R}\boldsymbol{i}_\mathrm{s} - (\hat{\alpha}\mathbf{I} - \hat{\omega}_\mathrm{m}\mathbf{J})\hat{\boldsymbol{\psi}}_\mathrm{R} \tag{14}$$

where $\hat{\alpha} = \hat{R}_\mathrm{R}/\hat{L}_\mathrm{M}$ is the estimate of the inverse rotor time constant. The estimated stator frequency is denoted by $\hat{\omega}_\mathrm{s}$. The rotor flux is estimated by

$$\frac{\mathrm{d}\hat{\boldsymbol{\psi}}_\mathrm{R}}{\mathrm{d}t} + \hat{\omega}_\mathrm{s}\mathbf{J}\hat{\boldsymbol{\psi}}_\mathrm{R} = \boldsymbol{e} + \boldsymbol{K}(\hat{\boldsymbol{e}} - \boldsymbol{e}) \tag{15}$$

where $\boldsymbol{K}$ is the gain matrix. In order to achieve an inherently sensorless observer, the gain is selected as

$$\boldsymbol{K} = \frac{\boldsymbol{G}\hat{\boldsymbol{\psi}}_\mathrm{R}\hat{\boldsymbol{\psi}}_\mathrm{R}^\mathrm{T}}{\|\hat{\boldsymbol{\psi}}_\mathrm{R}\|} \tag{16}$$

where $\boldsymbol{G} = g_1\mathbf{I} + g_2\mathbf{J}$. The classical approach of mimicking the current model at low speeds and the voltage model at high speeds is used: the details on the selection of the gains g_1 and g_2 can be found in [21]. The speed estimate is obtained from

$$\hat{\omega}_\mathrm{m} = \hat{\omega}_\mathrm{s} - \frac{\hat{R}_\mathrm{R}\boldsymbol{i}_\mathrm{s}^\mathrm{T}\mathbf{J}\hat{\boldsymbol{\psi}}_\mathrm{R}}{\|\hat{\boldsymbol{\psi}}_\mathrm{R}\|^2} \tag{17}$$

IV. Inductance Adaptation

A. Adaptation of Inverse-Γ Inductances

The inductances L_M and L_σ vary due to the magnetic saturation and are, thus, dependent on the operating point. A straightforward way to take into account the magnetic saturation would be to apply adaptation laws based on the back EMF according to

$$\frac{\mathrm{d}\hat{L}_\mathrm{M}}{\mathrm{d}t} = \boldsymbol{k}_\mathrm{M}^\mathrm{T}(\hat{\boldsymbol{e}} - \boldsymbol{e}), \quad \frac{\mathrm{d}\hat{L}_\sigma}{\mathrm{d}t} = \boldsymbol{k}_\sigma^\mathrm{T}(\hat{\boldsymbol{e}} - \boldsymbol{e}) \tag{18}$$

where the gain vectors are denoted by $\boldsymbol{k}_\mathrm{M}$ and $\boldsymbol{k}_\sigma$. However, a continuous adaptation of the inductances might lead to poor dynamics as fast variations in the currents or fluxes lead to fast variations in the inductances. Furthermore, when no speed sensor is used, there is not enough information to simultaneously estimate the value of both the leakage inductance and the magnetizing inductance. As a change in the flux level leads to variations in both inductances, one of the estimates would be inaccurate if the adaptation laws (18) would be applied. Moreover, the estimate of L_σ is very sensitive to parameters errors when the identification is based on fundamental-wave operating-point data as in (18), cf. [15].

B. Adaptation of Magnetic Saturation Function

Instead of adapting the inductances of the inverse-Γ model, the parameters of the stator inductance function (11) related to the Γ model are estimated. The function includes three parameters L_su, β, and S. For L_su and β, the adaptation laws

$$\frac{\mathrm{d}\hat{L}_\mathrm{su}}{\mathrm{d}t} = \boldsymbol{k}_\mathrm{L}^\mathrm{T}(\hat{\boldsymbol{e}} - \boldsymbol{e}), \quad \text{if } \psi_\mathrm{s} < \psi_\Delta \tag{19a}$$

$$\frac{\mathrm{d}\hat{\beta}}{\mathrm{d}t} = \boldsymbol{k}_\beta^\mathrm{T}(\hat{\boldsymbol{e}} - \boldsymbol{e}), \quad \text{if } \psi_\mathrm{s} > \psi_\Delta \tag{19b}$$

are proposed, where $\boldsymbol{k}_\mathrm{L}$ and $\boldsymbol{k}_\beta$ are the gain vectors for the parameters L_su and β, respectively. At low flux levels, the stator inductance is approximately equal to L_su while the parameter β has basically no influence on the inductance. As both parameters cannot be estimated simultaneously, a natural choice is to estimate L_su at flux levels below a flux limit ψ_Δ and β above the flux limit ψ_Δ. The parameter adaptation should not be coupled with the speed estimation. Therefore, the vectors are chosen as

$$\boldsymbol{k}_\mathrm{L} = k_\mathrm{L}\hat{\boldsymbol{\psi}}_\mathrm{R}/\|\hat{\boldsymbol{\psi}}_\mathrm{R}\| \tag{20a}$$

$$\boldsymbol{k}_\beta = k_\beta\hat{\boldsymbol{\psi}}_\mathrm{R}/\|\hat{\boldsymbol{\psi}}_\mathrm{R}\| \tag{20b}$$

where k_L and k_β are the adaptation gains. The stability analysis of the adaptation algorithm is presented in the Appendix. The resulting stability conditions for the adaptation gains are

$$k_\mathrm{L} < 0, \quad k_\beta > 0 \tag{21}$$

at stator frequencies above ω_Δ, cf. [21], which is the transition frequency between the current model and the voltage model in the observer. At lower speeds, it is advisable to turn the adaptation mechanism off.

The exponent S could also be adapted in a similar manner. However, there is often a priori information about the value of S [17]. Furthermore, the implementation is simpler if the exponent is an integer. The parameter S is, therefore, kept constant. The derivative of the stator inductance with respect to S is

$$\frac{\mathrm{d}L_\mathrm{s}}{\mathrm{d}S} = -\frac{L_\mathrm{su}(\beta\psi_\mathrm{s})^S \ln(\beta\psi_\mathrm{s})}{[1 + (\beta\psi_\mathrm{s})^S]^2} \tag{22}$$

which equals zero when $\psi_\mathrm{s} = 1/\beta$. The parameter β should, thus, be estimated at this flux level to minimize the influence of a possibly erroneous value of S. After finding the values of L_su and β, the exponent S could be tuned based on the estimate of β. If the estimate of β varies as a function of the flux level, the value of S is probably inaccurate.

C. Leakage Inductance Identification

An estimate $\hat{L}_\sigma$ of the chord-slope leakage inductance is necessary in the implementation of the proposed stator inductance identification method. As previously mentioned, the leakage inductance estimate becomes very sensitive to parameter errors if the identification is based on fundamental-wave data. Therefore, signal injection at a frequency higher than the fundamental frequency is used in order to identify the leakage inductance of the inverse-Γ model.

The identification is based on a simplified small-signal model presented in [22], and the principle of the identification method is the same as in [23], but here, a current signal is injected instead of a voltage signal. At higher frequencies, the relation between the stator voltage deviations and the stator current deviations can be modelled using a small-signal impedance matrix according to

$$\begin{bmatrix} u_\mathrm{sd}(s) \\ u_\mathrm{sq}(s) \end{bmatrix} = \begin{bmatrix} Z_\mathrm{dd}(s) & Z_\mathrm{dq}(s) \\ Z_\mathrm{qd}(s) & Z_\mathrm{qq}(s) \end{bmatrix} \begin{bmatrix} i_\mathrm{sd}(s) \\ i_\mathrm{sq}(s) \end{bmatrix} \tag{23}$$

Due to magnetic saturation, the machine appears to be salient in transients, and the inequalities $Z_\mathrm{dd}(s) \neq Z_\mathrm{qq}(s)$ and $Z_\mathrm{dq}(s) \neq -Z_\mathrm{qd}(s)$ hold. When identifying the leakage inductance, the saliency needs to be taken into account as the inductance estimate obtained depends on the direction of the injected signal. The direction that should be used to obtain the operating-point value of the inductance is not known in advance, and, therefore, the entire small-signal impedance matrix is measured.

In the estimated rotor-flux oriented reference frame, a high-frequency component is first superimposed on the d-direction current reference according to

$$i_\mathrm{sd,ref} = i_\mathrm{sd,f} + i_\mathrm{c}\sin(\omega_\mathrm{c}t) \tag{24}$$

where $i_\mathrm{sd,f}$ is the fundamental component reference, i_c the amplitude of the high-frequency current, and ω_c the angular frequency of the injected signal. The high-frequency component is extracted from the measured current by means of a discrete Fourier transform (DFT), and the obtained current phasor is denoted by $\underline{I}_\mathrm{d1}$. The corresponding voltage signal in the d direction is denoted by $\underline{U}_\mathrm{d1}$ and in the q direction by $\underline{U}_\mathrm{q1}$. As the current in the d direction oscillates, the rotor flux also starts to oscillate. The speed controller tries to keep the speed constant, and a small deviation in the q-direction current can, therefore, be observed. This deviation is denoted

by $\underline{I}_{\mathrm{q1}}$. The relation between the currents and voltages can be described by

$$\begin{cases} \underline{Z}_{\mathrm{dd}}\underline{I}_{\mathrm{d1}} + \underline{Z}_{\mathrm{dq}}\underline{I}_{\mathrm{q1}} = \underline{U}_{\mathrm{d1}} \\ \underline{Z}_{\mathrm{qd}}\underline{I}_{\mathrm{d1}} + \underline{Z}_{\mathrm{qq}}\underline{I}_{\mathrm{q1}} = \underline{U}_{\mathrm{q1}} \end{cases} \tag{25}$$

Next, the high-frequency component is superimposed on the q-direction current

$$i_{\mathrm{sq,ref}} = i_{\mathrm{sq,f}} + i_{\mathrm{c}} \sin(\omega_{\mathrm{c}} t) \tag{26}$$

In the frequency domain, the q-direction current is now denoted by $\underline{I}_{\mathrm{q2}}$. The corresponding voltage signals are denoted by $\underline{U}_{\mathrm{d2}}$ and $\underline{U}_{\mathrm{q2}}$ in the d and q direction, respectively, and the d-direction current is denoted by $\underline{I}_{\mathrm{d2}}$. The following equations now hold

$$\begin{cases} \underline{Z}_{\mathrm{dd}}\underline{I}_{\mathrm{d2}} + \underline{Z}_{\mathrm{dq}}\underline{I}_{\mathrm{q2}} = \underline{U}_{\mathrm{d2}} \\ \underline{Z}_{\mathrm{qd}}\underline{I}_{\mathrm{d2}} + \underline{Z}_{\mathrm{qq}}\underline{I}_{\mathrm{q2}} = \underline{U}_{\mathrm{q2}} \end{cases} \tag{27}$$

The impedance matrix can be obtained by solving the two systems of equations in (25) and (27). For simplicity, the voltages and current are extracted by using DFT in this paper. A faster identification could be achieved by applying a dual-reference-frame current controller for the injected signal [24]. The impedance matrix could also be obtained by using rotating current signal injection and analysing the clockwise and counter-clockwise components [25], [26].

Under the assumption that only the rotor leakage inductance saturation affects the small-signal characteristics at high frequencies, the leakage inductance seen in the rotor flux reference frame is [23]

$$L_\sigma = \mathrm{Im}\{\underline{Z}_{\mathrm{dd}}\}/\omega_{\mathrm{c}} \tag{28}$$

However, the saturation in the magnetizing inductance, and the mutual saturation between the magnetizing branch and the rotor branch also affect the high-frequency characteristics, and the inductance in (28) does not necessarily correspond to the desired operating-point inductance. In order to find the estimate for the chord-slope inductance, a coordinate transformation is applied. The inductance seen in a reference frame having the angle ϑ_0 with respect to the original rotor-flux oriented reference frame can be written as

$$\begin{aligned} L_\sigma(\vartheta_0) = \mathrm{Im}\big\{ &\underline{Z}_{\mathrm{dd}} \cos^2(\vartheta_0) + \underline{Z}_{\mathrm{qq}} \sin^2(\vartheta_0) \\ &+ \big(\underline{Z}_{\mathrm{dq}} + \underline{Z}_{\mathrm{qd}}\big) \cos(\vartheta_0)\sin(\vartheta_0) \big\} / \omega_{\mathrm{c}} \end{aligned} \tag{29}$$

The angle ϑ_0 is illustrated in Fig. 3, and the value of this angle is varied in the range of 0° to 180° when evaluating (29). As an example, the impedance matrix was measured at two different load levels, and the leakage inductance (29) is shown as a function of the angle in Fig. 4. As explained in [23], the maximum value of (29) corresponds to the best estimate of the leakage inductance. As the load torque increases, the leakage inductance decreases, and the leakage inductance identification has to be performed separately for every load level.

V. Implementation

The observer is implemented in the estimated rotor-flux coordinates. The equations for the rotor flux and stator frequency become

$$\frac{\mathrm{d}\hat{\psi}_{\mathrm{R}}}{\mathrm{d}t} = e_{\mathrm{d}} + g_1(\hat{e}_{\mathrm{d}} - e_{\mathrm{d}}) \tag{30}$$

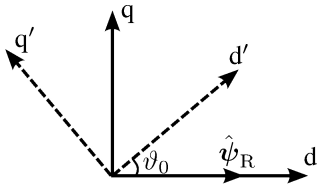

Fig. 3. Reference frames used in the identification of the leakage inductance. The inductance is first measured in the dq reference frame using signal injection. By means of a coordinate transformation, the inductance is calculated in the d′q′ reference frame as a function of ϑ_0.

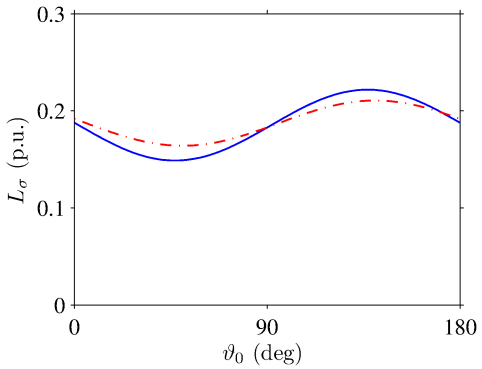

Fig. 4. Leakage inductance $L_\sigma(\vartheta_0)$ at two different load levels. The blue solid line is obtained at no load and the red dash-dotted line at 10% of the rated torque. The rotor flux is 0.3 p.u.

$$\hat{\omega}_{\mathrm{s}} = \frac{e_{\mathrm{q}} + g_2(\hat{e}_{\mathrm{d}} - e_{\mathrm{d}})}{\hat{\psi}_{\mathrm{R}}} \tag{31}$$

where

$$e_{\mathrm{d}} = u_{\mathrm{sd}} - \hat{R}_{\mathrm{s}} i_{\mathrm{sd}} - \hat{L}_\sigma \frac{\mathrm{d}i_{\mathrm{sd}}}{\mathrm{d}t} + \hat{\omega}_{\mathrm{s}} \hat{L}_\sigma i_{\mathrm{sq}} \tag{32a}$$

$$e_{\mathrm{q}} = u_{\mathrm{sq}} - \hat{R}_{\mathrm{s}} i_{\mathrm{sq}} - \hat{L}_\sigma \frac{\mathrm{d}i_{\mathrm{sq}}}{\mathrm{d}t} - \hat{\omega}_{\mathrm{s}} \hat{L}_\sigma i_{\mathrm{sd}} \tag{32b}$$

and

$$\hat{e}_{\mathrm{d}} = \hat{R}_{\mathrm{R}}(i_{\mathrm{sd}} - \hat{\psi}_{\mathrm{R}}/\hat{L}_{\mathrm{M}}) \tag{33}$$

The adaptation laws of L_{su} and β are

$$\frac{\mathrm{d}\hat{L}_{\mathrm{su}}}{\mathrm{d}t} = k_{\mathrm{L}}(\hat{e}_{\mathrm{d}} - e_{\mathrm{d}}) \tag{34a}$$

$$\frac{\mathrm{d}\hat{\beta}}{\mathrm{d}t} = k_\beta(\hat{e}_{\mathrm{d}} - e_{\mathrm{d}}) \tag{34b}$$

In the back-EMF equations (32) and (33), estimates of the parameters of the inverse-Γ model are used. The magnetizing inductance is calculated as $\hat{L}_{\mathrm{M}} = \hat{L}_{\mathrm{s}} - \hat{L}_\sigma$ where $\hat{L}_\sigma$ is the leakage inductance estimate obtained using signal injection. The stator inductance estimate $\hat{L}_{\mathrm{s}}$ is obtained from

$$\hat{L}_{\mathrm{s}} = \frac{\hat{L}_{\mathrm{su}}}{1 + (\hat{\beta}\hat{\psi}_{\mathrm{s}})^S} \tag{35}$$

where the stator flux amplitude is

$$\hat{\psi}_{\mathrm{s}} = \sqrt{(\hat{\psi}_{\mathrm{R}} + \hat{L}_\sigma i_{\mathrm{sd}})^2 + (\hat{L}_\sigma i_{\mathrm{sq}})^2} \tag{36}$$

The rotor resistance of the Γ model is assumed to be known, and the inverse-Γ rotor resistance is calculated using the model conversion given in (9). However, it is to be noted that the

rotor resistance does not have any influence on the inductance estimate as the parameters are obtained in steady state.

VI. Results

The performance of the adaptation algorithm was investigated by means of simulations and laboratory experiments on a 2.2-kW induction machine with the rated voltage 400 V, rated current 5 A, rated speed 1436 r/min, and rated torque 14.6 Nm. The machine is equipped with skewed and closed rotor slots. The value of the flux limit $\psi_\Delta = 0.45$ p.u., and the transition frequency $\omega_\Delta = 0.25$ p.u. The values of the adaptation gains were set to $k_\mathrm{L} = -5$ p.u. and $k_\beta = 1$ p.u. The performance of the adaptation algorithm is demonstrated at different speeds and loading conditions. Basically, it is enough to use only a few different flux levels, but here seven flux levels are used in order to get a good understanding of the adaptation method.

A. Simulation Results

The simulations were carried out in the MATLAB/Simulink environment, and the induction machine was implemented according to the Γ model. The following parameter values were used: $R_\mathrm{s} = 0.064$ p.u.; $R'_\mathrm{R} = 0.04$ p.u.; $L'_\sigma = 0.17$ p.u.; $L_\mathrm{su} = 2.31$ p.u.; $\beta = 0.87$ p.u.; and $S = 7$.

Fig. 5(a) shows the simulated result of the adaptation at the speed 0.75 p.u. as the value of the exponent S is known. No load is applied. At low flux levels, the value of $\hat{L}_\mathrm{su}$ converges rapidly to the actual value. When the flux is increased, the adaptation of $\hat{L}_\mathrm{su}$ is turned off and the parameter $\hat{\beta}$ is adapted instead. As seen in the figure, the parameter $\hat{\beta}$ converges also very fast to the actual value. The value of the estimated stator inductance (11) is at all flux levels very close to the actual value.

In Fig. 6, the influence of an erroneous value of the exponent S is demonstrated. The situation is similar to that in Fig. 5(a), but the value of the exponent is set to $S = 6$ instead of the actual value 7. At low flux levels, the influence of this error is very small, and the adaptation of $\hat{L}_\mathrm{su}$ is as good as in the previous case. At higher flux levels, however, the error in S makes the estimate $\hat{\beta}$ deviate from its actual value to compensate for the error in the exponent. Therefore, $\hat{\beta}$ varies as a function of the flux level and is no longer a constant. The resulting value of the estimated stator inductance is still very close to the actual inductance at all flux levels. However, if the value of $\hat{\beta}$ would be fixed to the value obtained at the highest flux level in Fig. 6, the error in the stator inductance would be about 3% at rated flux.

B. Experimental Results

In the laboratory experiments, the machine was fed by a frequency converter controlled by a dSPACE DS1103 PPC/DSP board. A servo motor was used as a load. Prior to the laboratory experiments, no-load tests were performed in order to obtain reference values for the parameters L_su, β, and S. The stator voltage and stator current were measured at different stator frequencies and voltage levels. The stator flux was evaluated at each operating point, and the stator inductance

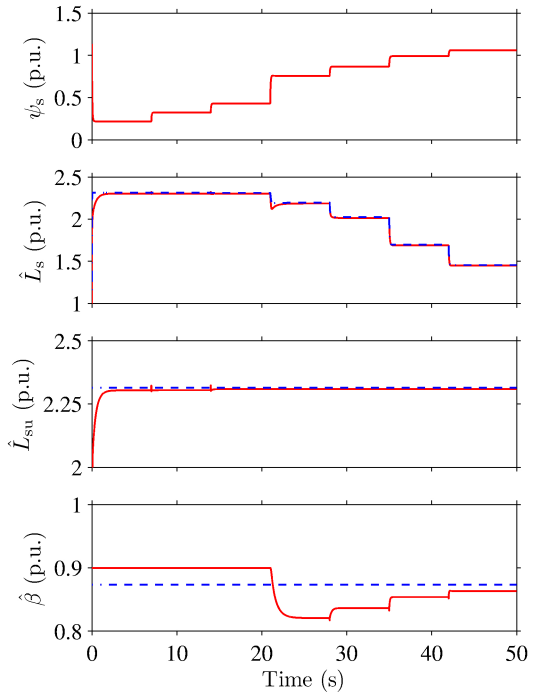

Fig. 6. Simulation results showing the adaptation of the saturation function parameters as the value of the exponent S deviates from the actual value. The rotation frequency is 0.75 p.u. and the load torque is zero.

function (11) was fitted to the data. The measured inductance values as well as the results of the data fitting are shown in Fig. 2. Before each measurement sequence, the leakage inductance was identified using signal injection, and the value at each flux level was stored in a look-up table. The injection frequency $\omega_\mathrm{c} = 2\pi \cdot 60$ rad/s and the amplitude of the injected signal was 0.02 p.u.

The experimental results in a no-load condition are shown in Fig. 5(b). The accuracy of the estimate of L_su is good as the rotor flux is 0.3 p.u. and 0.4 p.u., but at the lowest flux level of 0.2 p.u., the estimate is slightly lower than at the higher flux levels. A possible explanation is the presence of inaccuracies in the leakage inductance estimate. Theoretically, the leakage inductance has no influence at no load, but, due to mechanical losses, a true no-load condition cannot be achieved in practice. At very low flux levels, the q-direction current becomes relatively large and the sensitivity to inaccuracies in the leakage inductance estimate is high. Furthermore, the actual stator inductance decreases as a function of the load at low flux levels as can be seen in Fig. 2, and some decrease in $\hat{L}_\mathrm{su}$ is, therefore, expected.

In the experimental results, some ripple can be observed in the estimated parameters at the lowest and highest flux levels during the adaptation process. Due to this noise, the parameter estimates should be recorded for a short time and the mean value should be chosen as the final estimate. Fig. 7 shows the influence of the ripple on the speed and stator current. As the adaptation is activated only during the start-up of the drive, the ripple does not affect the actual dynamic performance. If desired, the ripple can be reduced by lowering the adaptation gains.

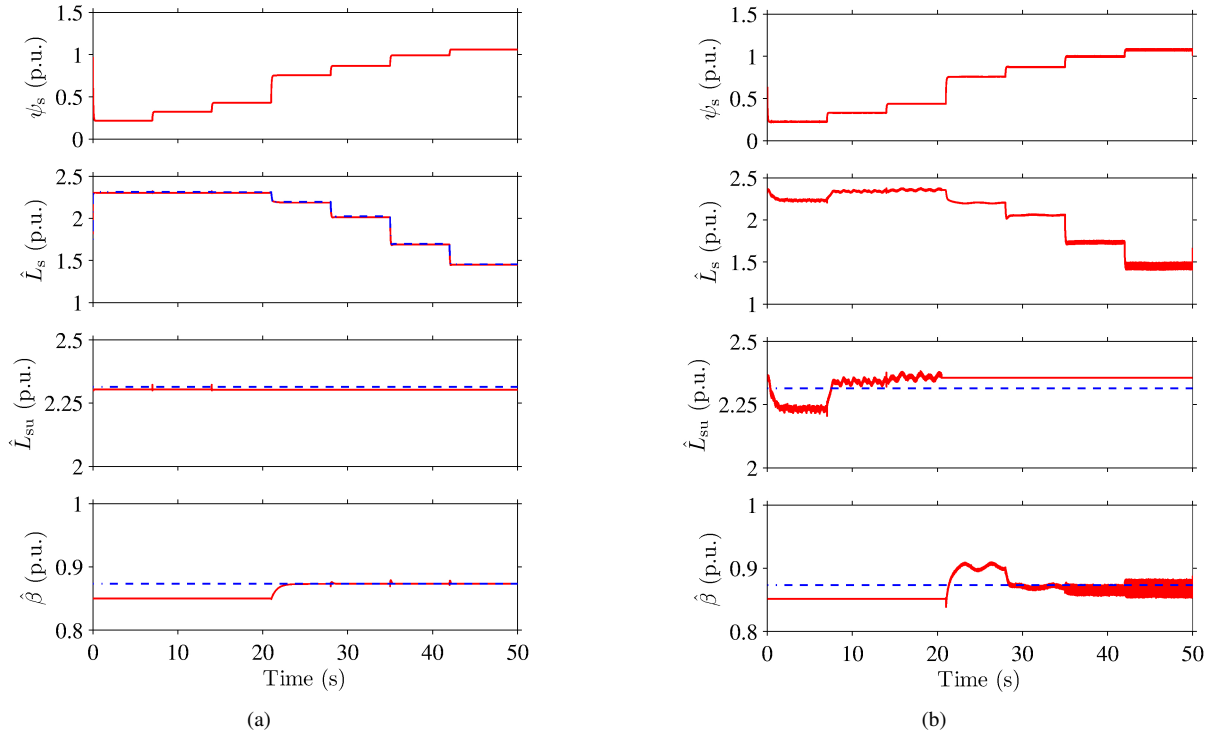

Fig. 5. Adaptation of the saturation function parameters without load from (a) simulations and (b) laboratory experiments. The rotation speed is 0.75 p.u. The uppermost subplot shows the stator flux, the second subplot shows the estimated stator inductance, the third subplot shows the estimated value of L_{su} and the last subplot the estimated value of β. Estimated values are shown by red solid lines. Blue dashed lines show (a) the actual values and (b) reference values from no-load tests.

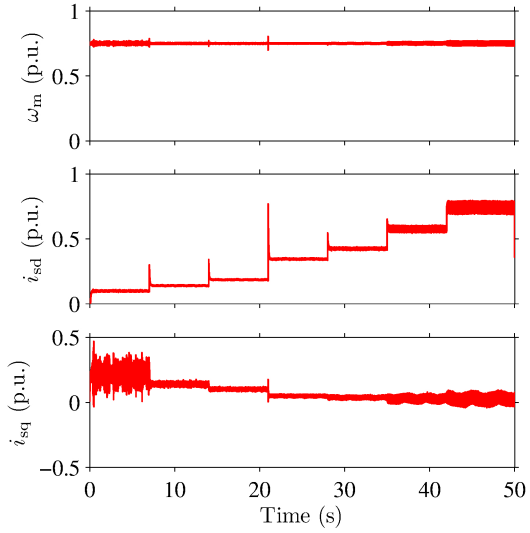

Fig. 7. Measured speed and current during the adaptation process in Fig. 5(b).

In the simulations, the results at low loads are practically identical to the results at no load. However, in the laboratory experiments, the estimate $\hat{L}_{\mathrm{su}}$ is very sensitive to inaccuracies in the leakage inductance $\hat{L}_\sigma$ at the lowest flux levels. An example is shown in Fig. 8, where 10% of the rated load is applied while the rotation speed is 0.5 p.u. The parameter $\hat{L}_{\mathrm{su}}$ can be successfully identified as the flux level is raised to 0.4 p.u. At high flux levels, the influence of a small load is negligible, and the accuracy of $\hat{\beta}$ is good. In order to further demonstrate the influence of the load, the measurement sequence of Fig. 5(b) is continued in Fig. 9 by applying torque steps of 20% of the rated torque as the rotor flux is constant at 0.8 p.u. As the load increases, the accuracy of $\hat{\beta}$ gradually decreases. As the rotor flux is kept constant, the stator flux increases with increasing load, cf. (36). The reduction seen in the stator inductance is mainly due to this increase in the stator flux amplitude.

The results at the rotation speed 0.15 p.u. are shown in Fig. 10. The adaptation gains were $k_{\mathrm{L}} = -2$ p.u. and $k_\beta = 0.2$ p.u. The accuracy of the adaptation is poorer at low speeds, and the estimate of L_{su} is about 5% too large. Due to the high value of $\hat{L}_{\mathrm{su}}$, the estimate $\hat{\beta}$ also increases as the rotor flux is about 0.7 p.u. At higher flux levels, the accuracy of $\hat{\beta}$ is still rather good. At this low speed, the influence of the leakage inductance estimate is negligible at all flux levels.

Based on the laboratory experiments, it is seen that the most accurate results are obtained when the speed is high and the load is sufficiently low. Very low flux levels should be avoided when identifying the parameter $\hat{L}_{\mathrm{su}}$ in order to minimise the influence of leakage inductance errors. The parameter $\hat{\beta}$ can successfully be identified if a flux level high enough is chosen. The minimum number of flux levels needed in the identification is two, and the model describing the entire saturation curve can, thus, be obtained in seconds or a few tens of seconds (depending on the machine size).

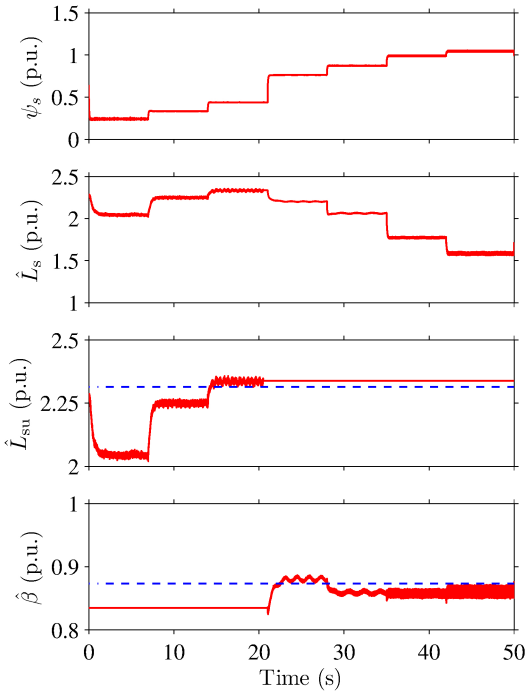

Fig. 8. Experimental results showing the adaptation of the saturation function parameters when a small load is applied. The rotation speed is 0.5 p.u. and the load torque is 10% of the rated load.

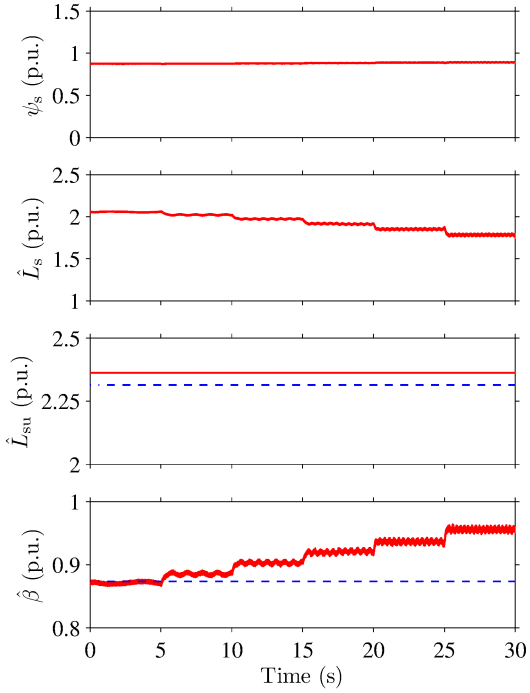

Fig. 9. Experimental results showing the adaptation of $\hat{\beta}$ as torque steps are applied. The rotor flux is kept constant at 0.8 p.u. and the rotation speed is 0.75 p.u.

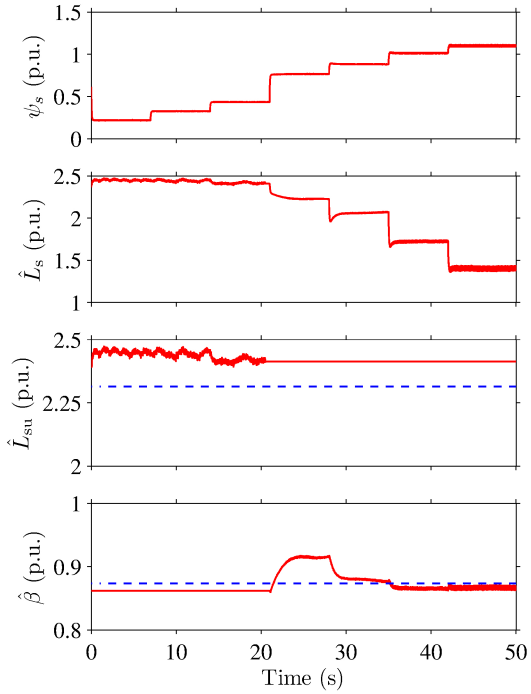

Fig. 10. Experimental results showing the adaptation of the saturation function parameters at the rotation speed 0.15 p.u.

VII. Conclusion

Due to the magnetic saturation, the inductances in the induction machine model are dependent on the operating point. In this paper, the magnetic saturation of the stator inductance was modelled by a power function. Adaptation laws for the parameters of the function were proposed. The entire magnetizing curve can be obtained in a short time by applying two flux levels (one just below the saturation point and one close to the rated flux). No additional data fitting method is necessary as the power function parameters are directly identified. Simulations and laboratory experiments show that the parameters can be estimated with good accuracy. The leakage inductance is identified by signal injection prior to the identification of the stator inductance. In this manner, good results are obtained even in non-ideal no-load conditions.

Appendix
Stability Analysis

Assuming constant L_{M}, L_σ and R_{R}, the nonlinear dynamics of the estimation error of L_{su} is

$$\frac{\mathrm{d}\tilde{L}_{\mathrm{su}}}{\mathrm{d}t} = \boldsymbol{k}_{\mathrm{L}}^{\mathrm{T}}(\hat{\boldsymbol{e}} - \boldsymbol{e}) \tag{37}$$

where $\tilde{L}_{\mathrm{su}} = \hat{L}_{\mathrm{su}} - L_{\mathrm{su}}$. The closed-loop system can be linearized as

$$\frac{\mathrm{d}}{\mathrm{d}t}\begin{bmatrix}\tilde{\boldsymbol{\psi}}_{\mathrm{R}} \\ \tilde{L}_{\mathrm{su}}\end{bmatrix} = \underbrace{\begin{bmatrix}\boldsymbol{A} & -B\boldsymbol{K}_0\boldsymbol{\psi}_{\mathrm{R0}} \\ -\boldsymbol{k}_{\mathrm{L}}^{\mathrm{T}}(\alpha\mathbf{I} - \omega_{\mathrm{m0}}\mathbf{J}) & -B\boldsymbol{k}_{\mathrm{L}}^{\mathrm{T}}\boldsymbol{\psi}_{\mathrm{R0}}\end{bmatrix}}_{\boldsymbol{A}'}\begin{bmatrix}\tilde{\boldsymbol{\psi}}_{\mathrm{R}} \\ \tilde{L}_{\mathrm{su}}\end{bmatrix} \tag{38}$$

where

$$\boldsymbol{A} = \begin{bmatrix}-g_{10}\alpha & -g_{10}\omega_{\mathrm{m0}} + \omega_{\mathrm{s0}} \\ -g_{20}\alpha - \omega_{\mathrm{s0}} & -g_{20}\omega_{\mathrm{m0}}\end{bmatrix} \tag{39}$$

$$B = -R_{\mathrm{R}}\frac{L_{\mathrm{su}}[1+(\beta\psi_{\mathrm{s0}})^S]+2L_\sigma[1+(\beta\psi_{\mathrm{s0}})^S]^2}{L_{\mathrm{su}}^3} \quad (40)$$

The system matrix is

$$\boldsymbol{A'} = \begin{bmatrix} -g_{10}\alpha & -g_{10}\omega_{\mathrm{m0}}+\omega_{\mathrm{s0}} & -g_{10}B\psi_{\mathrm{R0}} \\ -g_{20}\alpha-\omega_{\mathrm{s0}} & -g_{20}\omega_{\mathrm{m0}} & -g_{20}B\psi_{\mathrm{R0}} \\ -k_{\mathrm{L0}}\alpha & -k_{\mathrm{L0}}\omega_{\mathrm{m0}} & -k_{\mathrm{L0}}B\psi_{\mathrm{R0}} \end{bmatrix} \quad (41)$$

and the stability criteria then are

$$Bk_{\mathrm{L0}}\psi_{\mathrm{R0}}\omega_{\mathrm{s0}}^2 > 0 \quad (42)$$

$$\begin{array}{rcll} k_{\mathrm{L0}} & < & 0, & \text{if } c_0 > \omega_{\mathrm{s0}}^2 \\ k_{\mathrm{L0}} & > & -\frac{b_0 c_0}{B\psi_{\mathrm{R0}}(c_0-\omega_{\mathrm{s0}}^2)}, & \text{if } c_0 < \omega_{\mathrm{s0}}^2 \end{array} \quad (43)$$

The parameters b_0 and c_0 are positive in all operating points, and their definition can be found in [21].

The nonlinear dynamics of the estimation error of β is

$$\frac{\mathrm{d}\tilde{\beta}}{\mathrm{d}t} = \boldsymbol{k}_\beta^{\mathrm{T}}(\hat{\boldsymbol{e}}-\boldsymbol{e}) \quad (44)$$

The closed-loop system can be linearized as

$$\frac{\mathrm{d}}{\mathrm{d}t}\begin{bmatrix}\tilde{\boldsymbol{\psi}}_{\mathrm{R}} \\ \tilde{\beta}\end{bmatrix} = \underbrace{\begin{bmatrix}\boldsymbol{A} & -C\boldsymbol{K}_0\boldsymbol{\psi}_{\mathrm{R0}} \\ -\boldsymbol{k}_\beta^{\mathrm{T}}(\alpha\mathbf{I}-\omega_{\mathrm{m0}}\mathbf{J}) & -C\boldsymbol{k}_\beta^{\mathrm{T}}\boldsymbol{\psi}_{\mathrm{R0}}\end{bmatrix}}_{\boldsymbol{A''}}\begin{bmatrix}\tilde{\boldsymbol{\psi}}_{\mathrm{R}} \\ \tilde{\beta}\end{bmatrix} \quad (45)$$

where

$$C = R_{\mathrm{R}}S\beta^{S-1}\psi_{\mathrm{s0}}^S\frac{L_{\mathrm{su}}+2L_\sigma[1+(\beta\psi_{\mathrm{s0}})^S]}{L_{\mathrm{su}}^2} \quad (46)$$

$$\boldsymbol{A''} = \begin{bmatrix} -g_{10}\alpha & -g_{10}\omega_{\mathrm{m0}}+\omega_{\mathrm{s0}} & -g_{10}C\psi_{\mathrm{R0}} \\ -g_{20}\alpha-\omega_{\mathrm{s0}} & -g_{20}\omega_{\mathrm{m0}} & -g_{20}C\psi_{\mathrm{R0}} \\ -k_{\beta0}\alpha & -k_{\beta0}\omega_{\mathrm{m0}} & -k_{\beta0}C\psi_{\mathrm{R0}} \end{bmatrix} \quad (47)$$

The stability criteria are

$$Ck_{\beta0}\psi_{\mathrm{R0}}\omega_{\mathrm{s0}}^2 > 0 \quad (48)$$

$$\begin{array}{rcll} k_{\beta0} & > & 0, & \text{if } c_0 > \omega_{\mathrm{s0}}^2 \\ k_{\beta0} & < & -\frac{b_0 c_0}{C\psi_{\mathrm{R0}}(c_0-\omega_{\mathrm{s0}}^2)}, & \text{if } c_0 < \omega_{\mathrm{s0}}^2 \end{array} \quad (49)$$

ACKNOWLEDGEMENT

The authors gratefully acknowledge ABB Oy for the financial support.

REFERENCES

[1] A. Yahiaoui and F. Bouillault, "Saturation effect on the electromagnetic behaviour of an induction machine," *IEEE Trans. Magn.*, vol. 31, no. 3, pp. 2036–2039, May 1995.

[2] C. Gerada, K. Bradley, M. Sumner and P. Sewell, "Evaluation and modeling of cross saturation due to leakage flux in vector-controlled induction machines," *IEEE Trans. Ind. Appl.*, vol. 43, no. 3, pp. 694–702, May-June 2007.

[3] H. A. Toliyat, E. Levi and M. Raina, "A review of RFO induction motor parameter estimation techniques," *IEEE Trans. Energy Conv.*, vol. 18, no. 2, pp. 271–283, June 2003.

[4] M. Sumner and G. M. Asher, "Autocommissioning for voltage-referenced voltage-fed vector-controlled induction motor drives," *IEE Proc. B, Electr. Power Appl.*, vol. 140, no. 3, pp. 187–200, May 1993.

[5] H. Rasmussen and M. Knudsen and M. Tønnes, "Parameter estimation of inverter and motor model at standstill using measured currents only," in *Proc. IEEE ISIE'96*, vol. 1, Warsaw, Poland, June 1996, pp. 331–336.

[6] C. Sukhapap and S. Sangwongwanich, "Auto tuning of parameters and magnetization curve of an induction motor at standstill," in *Proc. IEEE ICIT'02*, vol. 1, Bangkok, Thailand, Dec. 2002, pp. 101–106.

[7] M. Ruff and H. Grotstollen, "Off-line identification of the electrical parameters of an industrial servo drive system," in *Conf. Rec. IEEE-IAS Annu. Meeting*, vol. 1, San Diego, California, Oct. 1996, pp. 213–220.

[8] N. R. Klaes, "Parameter identification of an induction machine with regard to dependencies on saturation," *IEEE Trans. Ind. Appl.*, vol. IA-29, no. 6, pp. 1135–1140, Nov./Dec. 1993.

[9] A. Gastli, "Identification of induction motor equivalent circuit parameters using the single-phase test," *IEEE Trans. Energy Conv.*, vol. 14, no. 1, pp. 51–56, March 1999.

[10] M. Bertoluzzo, G. S. Buja and R. Menis, "Self-commissioning of RFO IM drives: one-test identification of the magnetization characteristic of the motor," *IEEE Trans. Ind. Appl.*, vol. 37, no. 6, pp. 1801–1806, Nov./Dec. 2001.

[11] E. Levi and S. N. Vukosavic, "Identification of the magnetising curve during commissioning of a rotor flux oriented induction machine," *IEE Proc. Electr. Power Appl.*, vol. 146, no. 6, pp. 685–693, Nov. 1999.

[12] S.-I. Moon, A. Keyhani and S. Pillutla, "Nonlinear neural-network modeling of an induction machine," *IEEE Trans. Control syst. Technol.*, vol. 7, no. 2 pp. 203–211, Mar. 1999.

[13] E. Levi, M. Sokola and S. N. Vukosavic, "A method for magnetizing curve identification in rotor flux oriented induction machines," *IEEE Trans. Energy Conv.*, vol. 15, no. 2, pp. 157–162, June 2000.

[14] M. Wlas, Z. Krzemiński and H. A. Toliyat, "Neural-network-based parameter estimations of induction motors," *IEEE Trans. Ind. Elec.*, vol. 55, no. 4, pp. 1783-1794, April 2008.

[15] J. L. Zamora and A. García-Cerrada, "Online estimation of the stator parameters in an induction motor using only voltage and current measurements," *IEEE Trans. Ind. Appl.*, vol. 36, no. 3, pp. 805–816, May/June 2000.

[16] G. R. Slemon, "Modelling of induction machines for electric drives," *IEEE Trans. Ind. Appl.*, vol. 25, no. 6, pp 1126–1131, Nov./Dec. 1989.

[17] H. C. J. de Jong, "Saturation in electrical machines," in *Proc. ICEM'80*, vol. 3, Athens, Greece, Sept. 1980, pp. 1545–1552.

[18] S. Williamson and M. C. Begg, "Calculation of the bar resistance and leakage reactance of cage rotors with closed slots, *IEE Proc. B, Electr. Power Appl.*, vol. 132, no. 3, pp. 125–132, May 1985.

[19] M. Hinkkanen, A.-K. Repo and J. Luomi, "Influence of magnetic saturation on induction motor model selection," in *Proc. ICEM'06*, Chania, Greece, Sept. 2006.

[20] T. Tuovinen, M. Hinkkanen and J. Luomi, "Modeling of saturation due to main and leakage flux interaction in induction machines," *IEEE Trans. Ind. Appl.*, vol. 46, no. 3, pp. 937–945, May/June, 2010.

[21] M. Hinkkanen, L. Harnefors and J. Luomi, "Reduced-order flux observers with stator-resistance adaptation for speed-sensorless induction motor drives," *IEEE Trans. Power Electronics*, vol. 25, no. 5, pp. 1173–1183, May 2010.

[22] M. Hinkkanen, A.-K. Repo, M. Ranta and J. Luomi, "Small-signal modeling of mutual saturation in induction machines," *IEEE Trans. Ind. Appl.*, vol. 46, no. 3, pp. 965–973, May-June 2010.

[23] M. Ranta, M. Hinkkanen and J. Luomi, "Inductance identification of an induction machine taking load-dependent saturation into account," in *Proc. ICEM'08*, Vilamoura, Portugal, Sept. 2008.

[24] D. Basic, F. Malrait and P. Rouchon, "Current controller for low-frequency signal injection and rotor flux position tracking at low speeds," *IEEE Trans. Ind. Elec.*, vol. 58, no. 9, pp. 4010–4022, Sept. 2011.

[25] D. Raca, P. Garcia, D. Reigosa and R. Lorenz, "Carrier-signal selection for sensorless control of PM synchronous machines at zero and very low speeds," *IEEE Trans. Ind. Appl.*, vol. 46, no. 1, pp. 168–178, Jan./Feb. 2010.

[26] M. Linke, R. Kennel and J. Holtz, "Sensorless speed and position control of synchronous machines using alternating carrier injection," in *Proc. IEEE IEMDC'03*, Madison, WI, June 2003, pp. 1211–1217.

Mikaela Ranta received the M.Sc.(Eng.) degree from Helsinki University of Technology, Espoo, Finland, in 2006.

Since 2006, she has been with the Helsinki University of Technology (part of Aalto University, Espoo, since 2010). She is currently a Research Scientist with the Department of Electrical Engineering, Aalto University. Her main research interest is the modeling of electric machines.

Marko Hinkkanen (M'06) received the M.Sc.(Eng.) and D.Sc.(Tech.) degrees from the Helsinki University of Technology, Espoo, Finland, in 2000 and 2004, respectively.

Since 2000, he has been with the Helsinki University of Technology (part of Aalto University, Espoo, since 2010). He is currently an Assistant Professor with the Department of Electrical Engineering, Aalto University. His research interests include electric drives and electric machines.